Long Lasting ZnO Nanoparticle Synthesis for Potential Use in Inhalation Experiments

Moravec, Pavel
2015

LONG LASTING ZnO NANOPARTICLE SYNTHESIS FOR POTENTIAL USE IN INHALATION EXPERIMENTS

Pavel MORAVEC[1], Jaroslav KUPČÍK[1,2]

[1] Institute of Chemical Process Fundamentals of the CAS, v.v.i., Prague, Czech Republic, moravec@icpf.cas.cz
[2] Institute of Inorganic Chemistry of the CAS, v.v.i., Husinec-Řež, Czech Republic, kupcik@iic.cas.cz

Keywords: Chemical vapor synthesis, Nanoparticle generation, Chemical composition

INTRODUCTION

Zinc oxide nanoparticles (ZnO-NPs) exhibit unique chemical, optical and electrical properties due to their strong size and shape dependence. The applications of ZnO range from the UV emitting diodes to chemical sensors (Akgul *et al.*, 2013). Li *et al.* (2010) investigated the performance of ZnO nanoparticles (capped with aminopolysiloxane) in photodynamic therapy of cancer and reported the ability of ZnO nanoparticles to suppress the proliferation of cancer cells. Despite of increasing application of ZnO-NPs for industrial purposes, data about potential toxic properties are still rather rare and contradictory (Hackenberg *et al.*, 2011). In this work we tested the long term generation of ZnO-NPs for potential use in exposure experiments with laboratory animals. These experiments require the generation of NPs in the gas phase with appropriate number concentration (N_t>1×10^7 #/cm^3) and geometric mean diameter (GMD<50 nm) in duration of several weeks. Several methods of gas phase ZnO-NPs synthesis using metalorganic precursors, such as zinc acetylacetonate (Jensen *et al.*, 2000), zinc tetramethylheptane dionate (Brehm *et al.*, 2006), or diethylzinc (Ali *et al.* 2009) were reported in the literature. However, NPs prepared from metalorganic precursor are usually more or less contaminated by elemental (EC) or organic (OC) carbon (Moravec *et al.*, 2015). Therefore we used metallic zinc as a precursor in this study.

EXPERIMENTAL SETUP

Experiments were performed in an externally heated work tube with an i.d. 25 mm and 1 m-long heated zone. Total length of the work tube, made from impervious aluminous porcelain, was 1.5 m. Experimental set-up is described in more detail in Moravec *et* al. (2015). The boat with 4.3 g of zinc shot (Strem Chemicals, product No. 30-0070) was inserted into the middle of heating section. We used to call the work tube as a reactor, but in this arrangement it functioned as a saturator. The vapour pressure of zinc (P_{Zn}) was calculated from the equation from Wikipedia:

$$P_{Zn} = 133.32 \times 10^{\left(10.384 - \frac{6286}{T(k)}\right)},$$

valid above the melting point of zinc (419.5 °C). Carrier gas (nitrogen) saturated to some extent by Zn vapours – we do not expect saturation to the equilibrium – was mixed in the diluter with a stream of air, where oxidation of Zn vapours to zinc oxide was carried

out and the ZnO-NPs formation via gas-to-particle process occurred. Particle production in the form particle size distribution was monitored with scanning mobility particle sizer (SMPS, TSI model 3936L75) and the samples for particle characterization were deposited onto TEM grids using a nanometer aerosol sampler (NAS, TSI model 3089) and on cellulose and Sterlitech Ag filters. The particle characteristics were studied with high resolution transmission electron microscopy (HRTEM, *JEOL 3010*, Au or Ni TEM grids covered with C-foil), energy dispersive spectroscopy (EDS, *INCA/Oxford* connected to *JEOL 3010*, TEM grids), inductively coupled plasma – optical emission spectrometry (ICP-OES, *IRIS Intrepid II XDL*, cellulose filters) and X-ray diffraction (XRD, *Philips X'Pert diffractometer PW3020*, Ag filters). Interpretations of selected area electron diffraction (SAED) patterns were performed using program ProcessDiffraction (Lábár 2008; Lábár 2009). The particle production and characteristics were studied in dependence on reactor (saturator) temperature (T_R), and reactor (Q_R) and diluting (Q_{Dil}) flow rates.

RESULTS AND CONCLUSIONS

Besides preliminary experiments, two experimental campaigns with total duration more than 102 hours were performed. The particle production, expressed by N_t and GMD, in dependence on time and T_R, Q_R and Q_{Dil} during the first campaign is shown in Fig. 1. The particle production during first 48 scans was performed in an inert atmosphere, i.e. by evaporation/condensation method and N_t was low, cca 1×10^6 #/cm^3, even though T_R was as high as 600 °C. Introducing an air into the diluter at scan 49 and switching the process from evaporation/condensation to chemical vapour synthesis, the particle production increased considerably. After that, the particle production proceeded satisfactorily and can be controlled by adjusting experimental conditions: T_R=520-530 °C, Q_R=600-1000 cm^3/min, Q_{Dil}=1800-2200 cm^3/min.

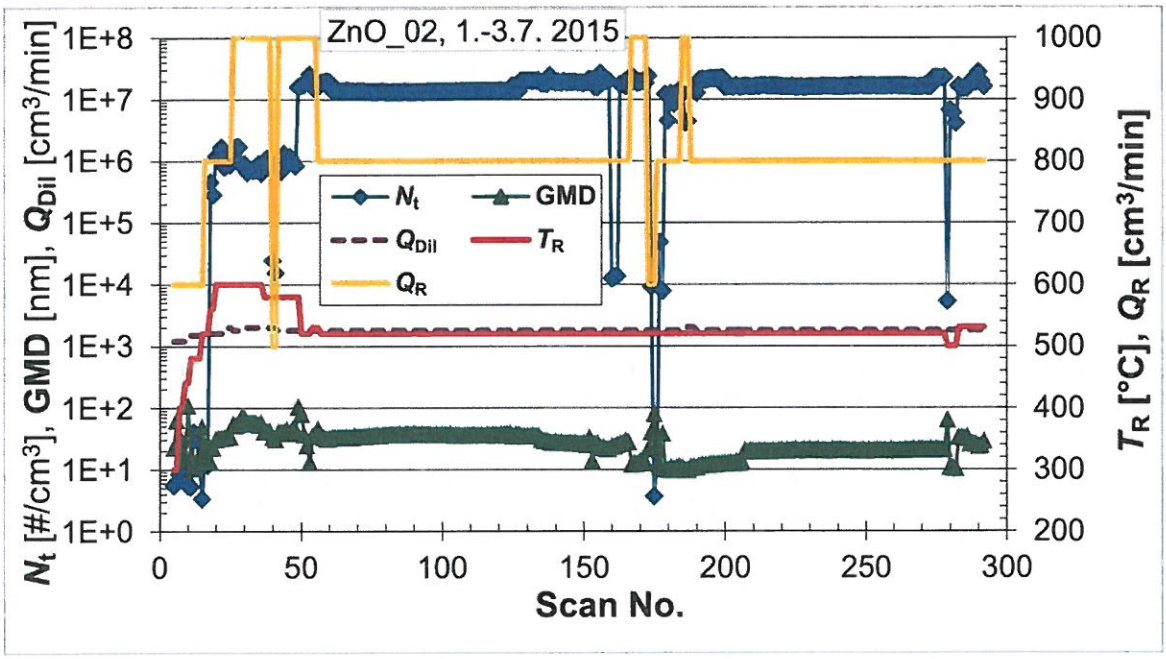

Fig. 1: Time dependence of N_t and GMD on time at given experimental conditions. 1 scan ~ 10 minutes.

Scans 160-161 and 279 represent sampling of the air from the laboratory and scans 175-179 show the restart of the process after a failure of the software (LabVIEW) controlling the electronic mass flow meters.

Morphology of NPs was studied using HRTEM and an example of HRTEM image can be seen in Fig. 2. Primary particles are mostly spherical, agglomerated into clusters of various sizes and the size of primary particles varies typically in the range from 10 to 20 nm.

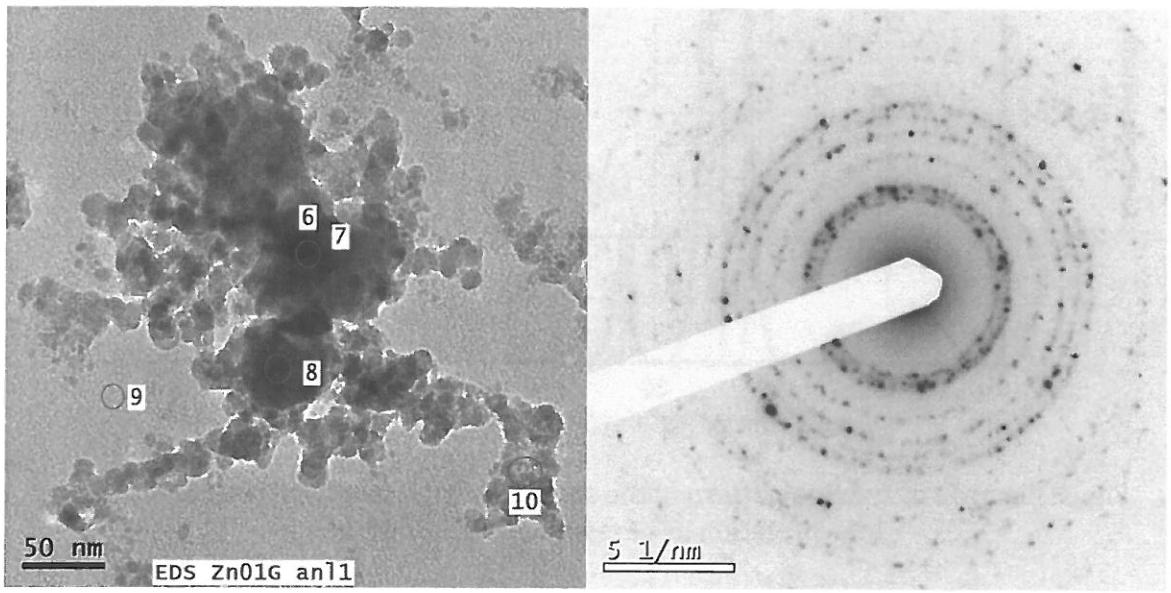

Fig. 2: TEM image and SAED pattern of the sample synthesized at T_R=520 °C, Q_R=800 cm^3/min and Q_{Dil}=1800 cm^3/min.

EDS analysis from the spot denoted as 6 and 7 showed 28 % of Zn (all results of EDS analysis are in atomic %), 42 % of O, 27 % of C and traces (1 % or less) of Au, Cu and Si. The composition of the spot 9 (TEM grid foil without deposit of NPs) is as follows: 90 % C, 8 % O and traces of Cu, Au and Zn. Here Cu, Au and most of C originates from TEM grid, some portion of C can also come from the atmosphere (CO_2 and hydrocarbons absorbed on the surface of NPs) and oxygen from NPs and partially from TEM grid foil. When we subtract the content O in spot 9 (8 %) from the value in spot 6 (42 %) the result is not far from the stoichiometric value for ZnO (28 %). ICP-OES analyses of three samples deposited on cellulose filters determined the content of ZnO in the samples as follows: 88, 89 and 69 weight %. In fact, we do not know why the third value (69 %) differs so much from the first (88 %) and the second (89 %). It might be possibly some error.

Crystallinity of NPs was studied by XRD and SAED. XRD analysis of four samples on Sterlitech Ag filters detected hexagonal ZnO crystalline phase in all samples, typically Pdf 89-0510. Mean crystallite size, calculated from the Scherrer equation, varied between 12.5 and 13.7 nm, crystallite sizes calculated by Pawley method were smaller; 7.5 – 10.9 nm. Comparing these values with typical NPs size in Fig. 2 we can see, that crystallite sizes are smaller than NPs, this means that NPs are not fully crystalline.

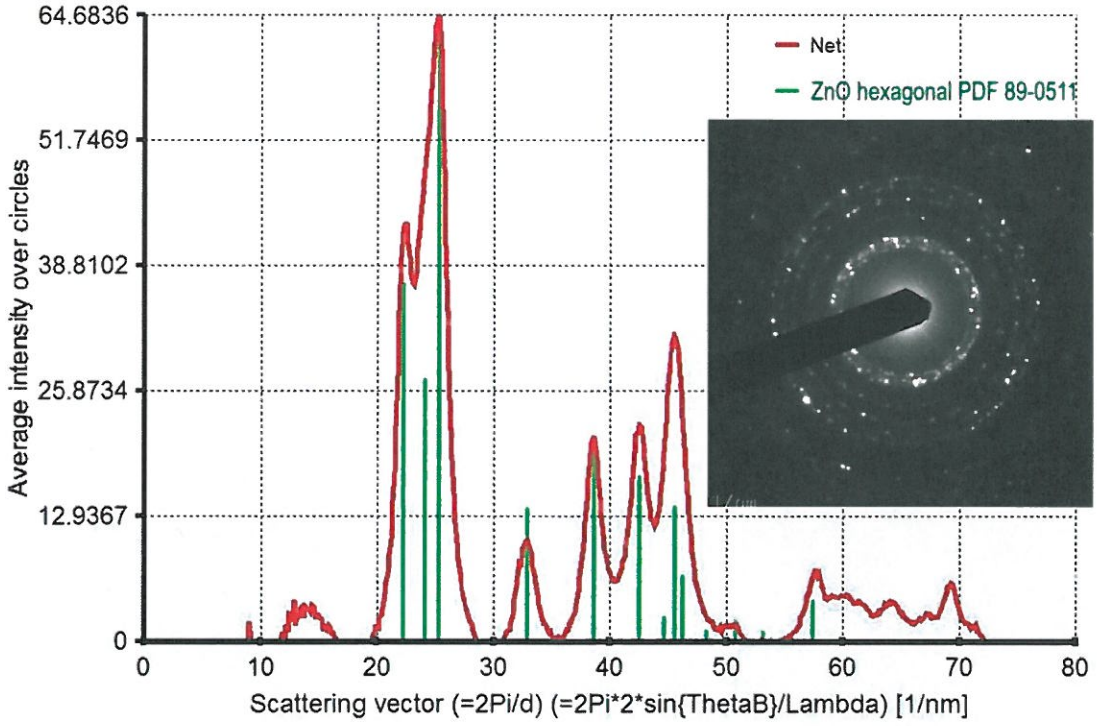

Fig. 3: Electron diffraction pattern of the sample Zn01G (inset and red curve) and its interpretation as hexagonal ZnO, Pdf 89-0511.

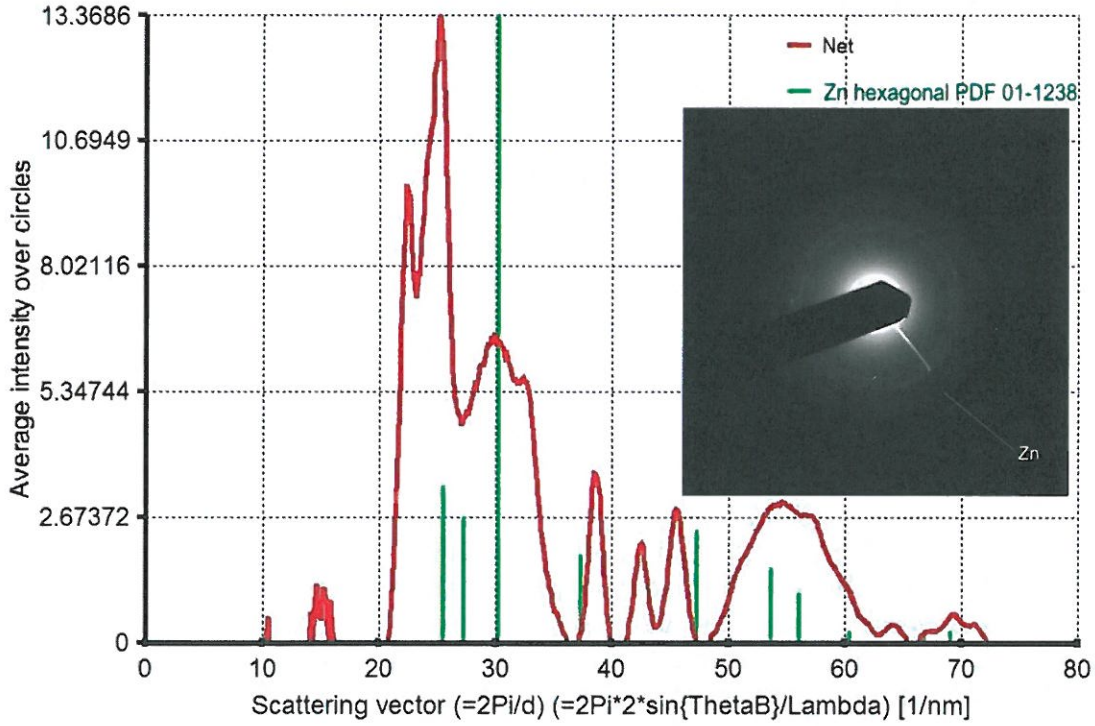

Fig. 4: Comparison of electron diffraction pattern of the sample Zn05G (inset and red curve) with model diffraction of hexagonal Zn, Pdf 01-1238.

Nearly identical results were obtained by SAED method, see Fig. 3. Electron diffraction pattern of the sample Zn01G is in very good agreements with model diffraction of hexagonal ZnO, Pdf 89-0511. Analogical results were obtained for most electron diffraction patterns taken by HRTEM from the samples Zn01G and Zn05G. However, in one electron diffraction pattern taken from the sample Zn05G a weak diffusion ring, which can be attributed to hexagonal Zn (Pdf 01-1238) is present, too. Other rings of the pattern fit with hexagonal ZnO, Pdf 05-0664. Nevertheless, this diffraction was rather weak and the ring corresponding to hexagonal Zn was on the detection limit of HRTEM, so that this result is hardly confirmative.

In conclusion, the method of evaporation of metallic zinc and subsequent oxidation of Zn vapours by a stream of air can generate ZnO-NPs of desired size and number concentration for sufficiently long time. Typical primary particle size varied between 10 and 20 nm, mean crystallite size of hexagonal ZnO, calculated by various methods, was in the range 7.5 – 13.9 nm. Concentration of ZnO in most samples reached almost 90 weight % and parameters of the particle production can be tailored by T_R, Q_R and Q_{Dil} as desired. Therefore, the method can be applied for long lasting exposure experiments with laboratory animals.

ACKNOWLEDGEMENT

This work was supported by the Czech Science Foundation under grant P503/12/G147. ICP-OES analyses were performed by Dr. Šárka Matoušková, Geological Institute of the CAS, v.v.i. and XRD analyses by Mgr. Anna Kallistová, Geological Institute of the CAS, v.v.i.

REFERENCES

Akgul, G., Akgul, F. a., Attenkofer, K., Winterer, M., Structural properties of zinc oxide and titanium dioxide nanoparticles prepared by chemical vapor synthesis, *J. Alloys&Compounds*, 554, 177-181 (2013).

Ali, M., Friedenberger, N., Spasova, M., Winterer, M. A Novel Approach for Chemical Vapor Synthesis of ZnO Nanocrystals: Optimization of Yield, Crystallinity, *Chem. Vap. Deposition*, 15, 192-198 (2009).

Brehm, J.U., Winterer, M., Hahn, H. Synthesis and local structure of doped nanocrystalline zinc oxides, *J. Appl. Phys.*, 100, 064311 (2006).

Jensen, J.R., Johannessen, T., Wedel, S., Livbjerg, H. Preparation of ZnO-Al_2O_3 particles in a premixed flame, *J. Nanoparticle Res.*, 2, 363-373 (2000).

Hackenberg, S., Scherzed, A., Technau, A., Kessler, M., Froelich, K., Ginzkey, C., Koehler, C., Burghartz, M., Hagen, R., Kleinsasser, N. Cytotoxic, genotoxic and pro-inflammatory effects of zinc oxide nanoparticles in human nasal mucosa cells in vitro, *Toxicology in vitro*, 25, 657-663 (2011).

Lábár, J.L. Electron diffraction based analysis of phase fractions and texture in nanocrystalline thin films; Part I: Principles, *Microscopy and Microanalysis* 14, 287-295 (2008).

Lábár, J.L. Electron diffraction based analysis of phase fractions and texture in nanocrystalline thin films; Part II: Implementation, *Microscopy and Microanalysis* 15, 20-29 (2009).

Li, J., Guo, D., Wang, X., Wang, H., Jiang, H., Chen, B. The photodynamic effect of different size ZnO nanoparticles on cancer cell proliferation in vitro, *Nanoscale Res. Lett.*, 5, 1063-1071 (2010).

Moravec, P., Smolik, J., Ondráček, J., Vodička, P., Fajgar, R. Lead and/or Lead Oxide Nanoparticle Generation for Inhalation Experiments, *Aerosol. Sci. Technol.* 49, 655-665 (2015).

https://en.wikipedia.org/wiki/Vapor_pressures_of_the_elements_(data_page)